

This is a repository copy of *The effect of grading the atomic number at resistive guide element interface on magnetic collimation*.

White Rose Research Online URL for this paper:

<https://eprints.whiterose.ac.uk/103720/>

Version: Accepted Version

Article:

Alraddadi, R. A B, Robinson, A. P L, Woolsey, N. C. orcid.org/0000-0002-2444-9027 et al. (1 more author) (2016) The effect of grading the atomic number at resistive guide element interface on magnetic collimation. *Physics of Plasmas*. 072706. ISSN 1089-7674

<https://doi.org/10.1063/1.4959037>

Reuse

Items deposited in White Rose Research Online are protected by copyright, with all rights reserved unless indicated otherwise. They may be downloaded and/or printed for private study, or other acts as permitted by national copyright laws. The publisher or other rights holders may allow further reproduction and re-use of the full text version. This is indicated by the licence information on the White Rose Research Online record for the item.

Takedown

If you consider content in White Rose Research Online to be in breach of UK law, please notify us by emailing eprints@whiterose.ac.uk including the URL of the record and the reason for the withdrawal request.

The effect of grading the atomic number at resistive guide element interface on magnetic collimation

R. A. B. Alraddadi,¹ A. P. L. Robinson,² N. C. Woolsey,¹ and J. Pasley^{1,2}

¹*York Plasma Institute, University of York, York YO10 5DD,
United Kingdom*

²*Central Laser Facility, STFC Rutherford-Appleton Laboratory, Didcot,
OX11 0QX, United Kingdom*

Using 3 dimensional numerical simulations, this paper shows that grading the atomic number and thus the resistivity at the interface between an embedded high atomic number guide element and a lower atomic number substrate enhances the growth of a resistive magnetic field. This can lead to a large integrated magnetic flux density, which is fundamental to confining higher energy fast electrons. This results in significant improvements in both magnetic collimation and fast-electron-temperature uniformity across the guiding. The graded interface target provides a method for resistive guiding that is tolerant to laser pointing.

I. INTRODUCTION

Plasma resistivity induces a significant magnetic field inside an overdense plasma when a shear in the fast electron current density or resistivity gradient exists. This is described by the induction equation in the hybrid approximation¹,

$$\frac{\partial \vec{B}}{\partial t} = \eta(\nabla \times \vec{j}_f) + (\nabla \eta) \times \vec{j}_f \quad (1)$$

where \vec{B} is the flux density of the magnetic field, η is the resistivity and \vec{j}_f is the fast electron current density. The first term on the right-hand side generates a magnetic field that directs electrons towards regions of higher current density, and thus, acts to collimate the fast electron beam. The second term, which forms the basis of resistive guiding concept^{2,3}, generates a magnetic field at resistivity gradients which acts to keep the fast electrons within regions of higher resistivity. The resistivity gradient is created by a transition between two materials with different atomic number Z . This can be in the form of high- Z solid wire (the guide) embedded in a lower- Z substrate⁴. The resistivity gradient is in transverse direction to that of the fast electron beam propagation. The fast electrons are generated within the guide and the magnetic field at the interface between this guide and the substrate (of lower Z material) will deflect the electrons and keep them inside the high- Z material.

The ability of a resistive guide to confine fast electrons depends on the ratio of the fast electron Larmor radius to the generated azimuthal magnetic field width L_ϕ . The confinement condition of the fast electrons along the guide is expressed as^{2,5},

$$B_\phi L_\phi \geq \frac{P_f}{e}(1 - \cos \theta_d) \quad (2)$$

where B_ϕ is the azimuthal magnetic flux density, $P_f = \gamma_f v_f m_e$ is the fast electron momentum, γ_f is the Lorentz factor, v_f is the fast electron velocity and θ_d is the fast electron divergence angle. This implies that the product of $B_\phi L_\phi$ needs to be larger than the fast electron momentum to reflect the fast electrons back towards the guide axis^{2,4}. For fast electrons entering the guide at an angle of $\theta_d = 30^\circ$ with energy of 1.8 MeV, a $B_\phi L_\phi$ of 10^{-3} Tm is needed for confinement. The product of $B_\phi L_\phi$ needs to be larger than this when either the entrance angle or the fast electron energy increases. For example, $B_\phi L_\phi$ has to be about $\approx 7 \times 10^{-3}$ Tm for 4.5 MeV fast electrons with angle of $\theta_d = 50^\circ$.

The resistive guide has been suggested for applications such as the Fast Ignition approach to the inertial confinement fusion scheme^{6,7} where the energetic fast electrons need to be guided through an overdense stand-off distance of 100 μm or more⁸ and deposited into the compressed core of DT plasma. It has been suggested that a resistive guide element can also be used as a driver in hydrodynamic experiments^{4,9} since strong heating occurs where the fast electron beam is collimated. Robinson *et al.*⁴ have investigated analytically and numerically the most significant parameters that affect the heating of the resistive guide element. They find for example, the ratio of the guide radius to the laser spot radius needs to be comparable in order to obtain good heating. In a real laser system, this condition is difficult to achieve due to the limitation of the laser pointing stability. If the laser hits the edge of the resistive guide element rather than its centre, the guide will not achieve its aim as a collimator and the fast electrons will couple into the substrate. Therefore, a larger radius guide is needed. However, numerical work^{4,9} shows that by using a larger radius guide magnetic fields develop within the guide close to its axis degrading heating uniformity. These “interior” magnetic fields are due to inhomogeneous propagation of the fast electrons¹⁰. They produce annular transport pattern which leads to preferential heating of the outer regions of the guide.

Hitherto, the resistive guide in all previous experimental^{11,12} and numerical^{4,9} studies has an engineered step-like atomic number interface between the guide and the substrate regardless of the guide geometry. We will refer to this configuration as “step-like” resistive guide configuration. Since the resistive magnetic field is produced at the guide-substrate interface, changing the interface resistivity away from a step-like interface offers a means to improve electron guiding and enable heating of a larger radius guide. We find that grading the atomic number across a layer at the guide-substrate interface (so that the atomic number, and thus the resistivity, decreases with increasing radius) enhances the growth of resistive magnetic field. This cladding layer can lead to a larger integrated magnetic flux density, which improves the magnetic collimation of the fast electrons. Furthermore, as a result of this, simulations show an improvement in radial heating uniformity in the larger radius guide.

This paper is structured as follows; Sec. II contains a description of the different resistive guide designs. Sec. III outlines the simulation set up and the simulation results and discussion are contained in Sec. IV and V respectively.

II. GRADING THE ATOMIC NUMBER AT THE INTERFACE OF THE GUIDE ELEMENT

To highlight the impact of a graded-interface, four simulations are reported. Two use a step-like interface (simulation A and B in Table 1) and two use shaped or graded interface (C and D in Table 1). The aim of these simulations is to compare the resulting magnetic collimation and radial temperature profiles in the guides. The guide is a cylindrical wire in all simulations as summarised in Table 1. r_{guide} is the total radius of the embedded guide while r_{core} is the radius of the core of the guide. The core has not been graded. χ is the ratio of the radius of the core r_{core} to the laser radius spot r_{spot} . It was found that for graded-interface targets that this ratio needs to be less than 1. When $\chi > 1$ the fast electron beam breaks into filaments inside the guide resulting in non-uniform radial heating of the guide.

Simulation	r_{guide}	r_{core}	r_{spot}	χ	Guide-substrate interface shape
	(μm)	(μm)	(μm)		(shown in Figures 2)
A	5	5	3.5	1.4	(a)
B	2.5	2.5	3.5	0.7	(b)
C	5	2.5	3.5	0.7	(c)
D	5	2.5	3.5	0.7	(d)

Table I: Table of guide geometric parameters

Figures 1 (a)-(d) show 2-dimension z-x plane slices of the target Z profile for targets A to D. These figures are taken in the mid y -direction at $-15 < z < 15$ along the x -direction. The materials used in simulations A and B are solid density (2.7 gcm^{-3}) aluminium guide ($Z = 13$) embedded into a solid (1.0 gcm^{-3}) CH plastic ($Z = 3.5$) substrate. The difference between simulations A and B is the guide radius, which is $5 \mu\text{m}$ and $2.5 \mu\text{m}$ respectively. The resistive guide design in simulation C (Figure 1(c)) is an Al guide clad in a carbon (density 2.2 gcm^{-3}) layer. This resembles a co-axial cable design. We refer to this design as “co-axial ” resistive guide and the overall radius of this co-axial guide is $5 \mu\text{m}$. Simulation D, Figure 1(d), uses an Al guide of radius $2.5 \mu\text{m}$ clad in a graded layer of material of linearly decreasing Z from $Z= 6$ to $Z = 3.5$ between radial positions of $2.5 \mu\text{m}$ and $5 \mu\text{m}$. The overall radius of the guide (with cladding) is $5 \mu\text{m}$. This is embedded in a CH plastic substrate. The radial atomic number profiles are shown in Figures 2 (a)- (d). The fast electrons are

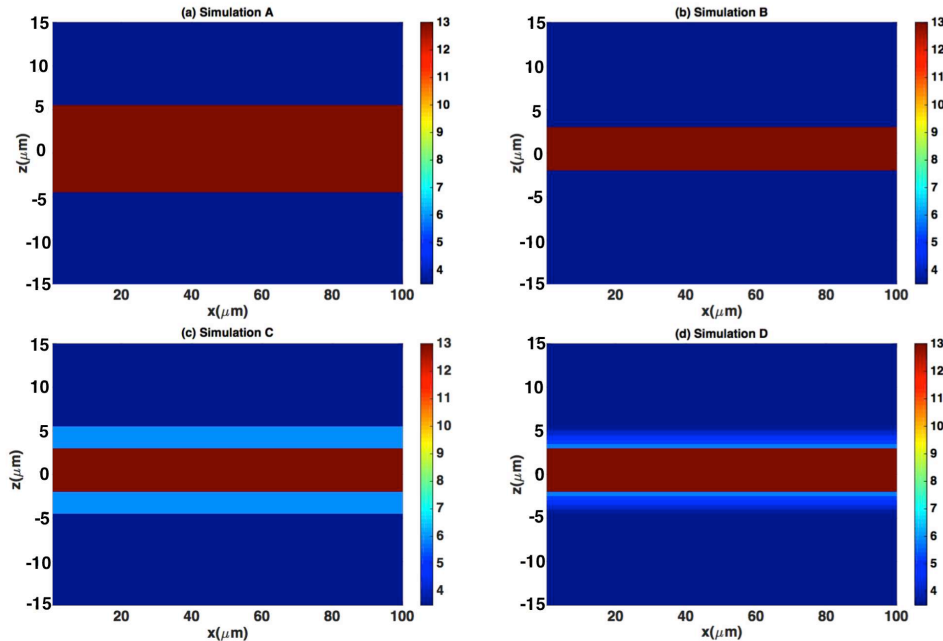


Figure 1: Figures (a)-(d) show the target Z profile for simulations A to D respectively. Simulations A and B use a step-like interface and the difference between the two is only in the guide radius. Simulation C use a shaped interface resembling a co-axial cable design. Simulation D uses the graded interface resistivity cladding guide.

injected into the guide from the left hand side at $x = 0$ and the centre of y and z .

III. SIMULATION SET UP

The simulations were performed using the 3 dimensional particle hybrid code ZEPHYORS^{4,13} which is based on the hybrid method developed by Davies in a series of publications^{13,14}. ZEPHYORS is used to simulate the 3D relativistic motion of electrons under the influence of self-generated resistive electric and magnetic fields, as well as collisions. The fast electron current \vec{j}_f propagate into the plasma when it is spatially coincident and nearly-balanced with cold return electron current \vec{j}_r that is drawn from the background¹⁵, i.e. $\vec{j}_f \approx -\vec{j}_r$. The resistive electric field is estimated from Ohm's law, $E = -\eta\vec{j}_f$, with displacement current dropped from Amp'ere's law. Ignoring displacement current relies on the assumption that the change in the electric field with time is slow. This is valid since the width of the beam, i.e. the fast electron bunch radius, is much smaller than the length of the fast electron bunch. In addition, the electron pressure term ($-\nabla P_e/n_e$) is also neglected in Ohm's law. The

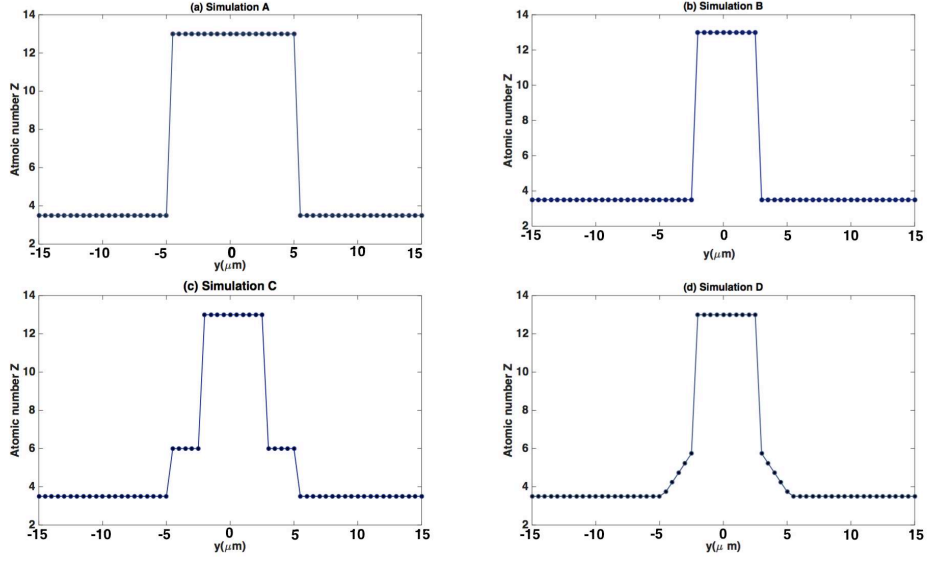


Figure 2: Figures (a)-(d) show the radial atomic number profile for simulations A to D respectively. Simulations A and B use Aluminium guide. Simulation C uses an Al guide clad in a carbon layer. Simulation D uses an Al guide clad in a graded layer of material of linearly decreasing Z. All the guides are embedded into the CH plastic substrate.

reason for this is the contribution of the electric field from this term is small by about two orders of magnitude compared to the electric field that obtained from resistive term. Thus, from Faraday's law the resulting resistive magnetic field arising due to the fast electrons can be written as (1). The return electron current heats the background plasma, via Ohmic heating, with power density $\vec{j}_r \cdot E \approx \eta j_f^2$. The background electrons are treated as a static fluid that experience heating, ionisation and change in resistivity. The static treatment of the background is reasonable as the hydrodynamic displacement is about $0.1 \mu\text{m}$ in 1 ps for targets heated to 100 eV, assuming that the sound speed is 10^5 m/s . Thomas-Fermi model is used to obtain the ionisation and specific heat capacity of the background. The resistivity is temperature dependent and based on that of Lee and More resistivity model¹⁶. The temperature is calculated by the energy deposition due to the slowing down of the fast electrons and the Ohmic heating induced by the return electron current. The fast electron population is described kinetically using the Vlasov equation, which is solved via the PIC method. Collisions are included using the Fokker-Planck collisional operators, which account for angular fast electron scattering from background ions and electrons, together with drag

generated by the background electrons. The mathematical expressions of the collisional operators are obtained from Davies¹³ equations (1) and (2). More details about the physics of hybrid code can be found in Robinson *et al*⁸.

A $200 \times 100 \times 100$ grid was used with a $0.5 \mu\text{m}$ cell size in each direction. The number of macroparticles injected into each of the cells was 126. This helped to reduce statistical noise. The target, as described above, consisted of a CH plastic substrate within which a guide of radius r_{guide} was embedded. This guide is co-linear along the x -axis and centred on y and z as shown in Figures 1. The laser irradiation intensity was $1.27 \times 10^{20} \text{ Wcm}^{-2}$ with a pulse duration of 2 ps and the laser wavelength of $1 \mu\text{m}$. It is assumed that 30% of the laser energy was coupled to the fast electrons. The temporal profile of the fast electron beam is top-hat shaped and the transverse profile is $\propto \exp[-\frac{r^2}{2r_{\text{spot}}^2}]$, where $r_{\text{spot}} = 3.5 \mu\text{m}$. The choice of $r_{\text{spot}} = 3.5 \mu\text{m}$ was to ensure the electron beam source is within the resistive guide of $5 \mu\text{m}$. It worth mentioning that these choice of small sizes of both r_{spot} and r_{guide} were to minimise the simulation time. The fast electron angular distribution is uniform over a solid angle and defined by the half-angle of divergence 50° . The energy distribution of the fast electrons is from the reduced Wilks' ponderomotive scaling¹⁷, giving $T_f = 2.7 \text{ MeV}$ ¹⁸. The resistivity uses the Lee and More model and a minimum mean free path as $5r_s$, where r_s is interatomic spacing. From Table I, it can be seen that simulations A, C and D have total $r_{\text{guide}} > r_{\text{spot}}$ ensuring that the electron beam source is within the guide. This is not the case in simulation B where $r_{\text{guide}} < r_{\text{spot}}$. However, r_{core} in simulation B is identical to simulations C and D.

IV. RESULTS

A. The effect of design on the azimuthal magnetic field rate

Figures 3 (a)-(d) show an x - z slice taken at the mid-plane of y of the generated magnetic field at 2.2 ps for simulations A to D. Generally, an azimuthal magnetic field has been generated at the interface between the guide and the CH plastic substrate. This field provides collimation for the fast electrons. Radial expansion of the fast electron beam is evident from the formation of the magnetic field in the CH plastic substrate outside the guide. In simulation A (Figure 3(a)) magnetic field features are evident within the guide, these are

close to the axis and are most noticeable occurring between $x = 20 \mu\text{m}$ and $x = 40 \mu\text{m}$. Here the $r_{\text{guide}} > r_{\text{spot}}$ and χ is larger than 1. This “interior” magnetic field is due to the inhomogeneous propagation of the fast electrons¹⁰. The generation of these fields within the guide is undesirable and inhibits radially uniform fast electron heating.

Magnetic fields interior to the guide are not observed in simulations B, C and D where $\chi < 1$ although $r_{\text{guide}} > r_{\text{spot}}$ in simulations C and D. This implies that more uniformity of the fast electron propagation is obtained in these guides. In simulation C, the co-axial resistive guide, two azimuthal magnetic fields are observed, the first is between the guide and the CH plastic substrate at radial positions of $5 \mu\text{m}$ and the second is between the carbon cladding and the aluminium core, i.e. at radial position of $2.5 \mu\text{m}$. Because of this, the fast electrons are confined at three individual positions, between $-5 \mu\text{m}$ and $-2.5 \mu\text{m}$, $-2.5 \mu\text{m}$ and $+2.5 \mu\text{m}$ and $+2.5 \mu\text{m}$ and $+5 \mu\text{m}$ as shown in Figure 3(c). The azimuthal magnetic fields in simulations B and D shown in Figures 3 (b) and (d) respectively are similar although the total guide radius in simulation D is twice that in simulation B. In simulation D, the azimuthal magnetic field is generated along the graded region of the guide and located along the interface with the core of the guide. The observation that the magnetic flux density in simulation D is higher than that in simulation B, which has a step-like interface, by 10^3 T is notable and important. Simulation D also indicates that changing the interface shape does not significantly affect the width of the magnetic field.

Figure 4 shows the resulting product $B_\phi L_\phi$ as a function of time which is extracted at $x = 10 \mu\text{m}$, and in the y mid-plane for all the simulations. The product $B_\phi L_\phi$ is calculated from the peak of the magnetic field and the FWHM. Simulation D has the largest product $B_\phi L_\phi$ of all simulations and indicates that this guide can confine higher energy electrons. A high value of $B_\phi L_\phi$ (10^{-3} Tm at 200 fs in simulation D) is important to collimation of the fast electron beam and subsequent heating of the guide. Simulation B achieves a similar $B_\phi L_\phi$ by 300 fs however, since $r_{\text{guide}} < r_{\text{spot}}$ more fast electrons escape the guide and move into the CH plastic substrate. This reduces the $B_\phi L_\phi$ product further limiting the fast electron confinement. The $B_\phi L_\phi$ product in simulation C is inferior to that in simulation A as the fast electrons are confined in multiple regions of the guide as shown in Figure 3(c). Nevertheless, we find (see in Sec. IV B) that the radial heating within the guide in simulation C is more uniform than in simulation A. This is because electron beam filamentation is suppressed even in situation where a coaxial guide has higher current densities. In summary, a resistive

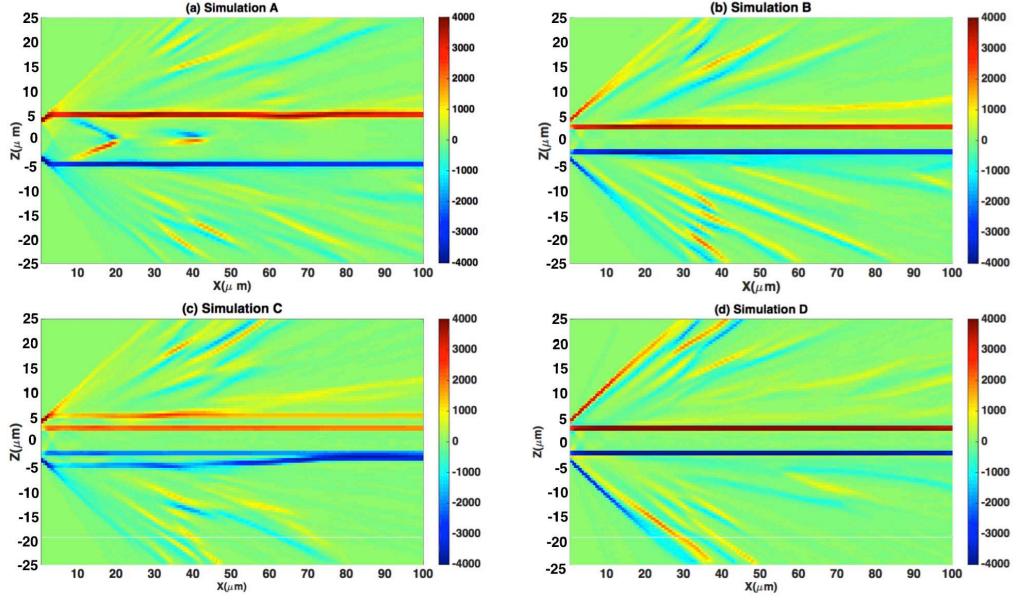


Figure 3: x - z slice of the magnetic field (T) in the y midplane at 2.2 ps for simulations A to D.

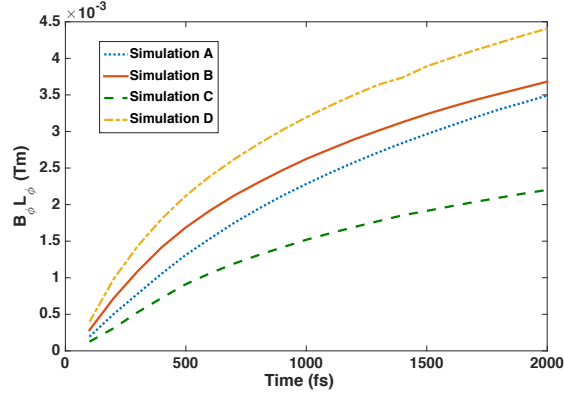


Figure 4: The product of $B_\phi L_\phi$ near the head of the beam $x = 10\mu\text{m}$ at different times in fs.

guide using a graded interface increases the magnetic flux density and produces a significantly larger $B_\phi L_\phi$ product. This enhances electron confinement.

B. The effect of design on the guide heating

Figure 5 shows an x - z slice of the background temperature in eV taken in the mid y -plane at 2.2 ps for simulations A to D. Strong resistive return current heating occurs in the guides

where the fast electrons are collimated. There is a gradient in temperature with depth along the guide (x -direction) which is observed in all simulations. However, this gradient differs in each simulation due to electron confinement which results from the differences in the generated azimuthal magnetic field. Non-uniform radial heating is observed in simulation A with striking annular temperature profiles at $x = 20 \mu\text{m}$ and $x = 40 \mu\text{m}$. This corresponds to the location of the interior magnetic field previously noted (see Figure 3(a)). More uniform heating is obtained in simulation B, this is due to the small radius of the guide and similar results are noted by Robinson *et al.*⁴. The heating in simulation B is comparable to simulation D which has twice the guide radius. This result is important and identifies a possible method for designing targets that are tolerant of laser pointing stability. The key is to increase the guide radius using a graded resistivity cladding. **The laser pointing stability in this design will be subject of future work as we will closely examine this in more detail.** The resulting guide has good radial temperature uniformity and relatively unstructured decrease in temperature along the depth. The resistivity grading between the guide core and plastic substrate with $\chi < 1$ ensures that the fast electrons with diverging trajectories are redirected towards the higher resistivity regions. Temperatures in simulation C is lower and more structured than in simulations B and D. This is expected based on the simulated $B_\phi L_\phi$. The temperature in simulation C is higher than in simulation A although the $B_\phi L_\phi$ product is lower. This results from the lack of internal magnetic field in co-axial target design.

Cross-section from Figure 5 are shown in Figure 6. These are taken at 2.2 ps along the guide depth at the centre of y and z axes. The effect of the internal magnetic field excluding fast electrons and leading to poor heating at $x = 20 \mu\text{m}$ and $x = 40 \mu\text{m}$ in the centre of the guide in simulation A is evident. An important comparison is between simulations B, C and D where $\chi < 1$. There is oscillation in their temperature profiles within $15 \mu\text{m}$ of the surface. This is due to inhomogeneity in the fast electron propagation near the injection region. After this, a gradual reduction in the temperature occurs. The differences in temperature between simulations B and D is due to the fact that that $r_{guide} > r_{spot}$ in simulation D while $r_{guide} < r_{spot}$ in simulation B.

It is worth mentioning that the fast electrons heat the resistive guide structure to high temperatures in few picoseconds. As discussed in Sec. III, the hydrodynamic motion becomes important on timescale of 10 to 30 ps and it should be negligible at time up to 1 to 3 ps.

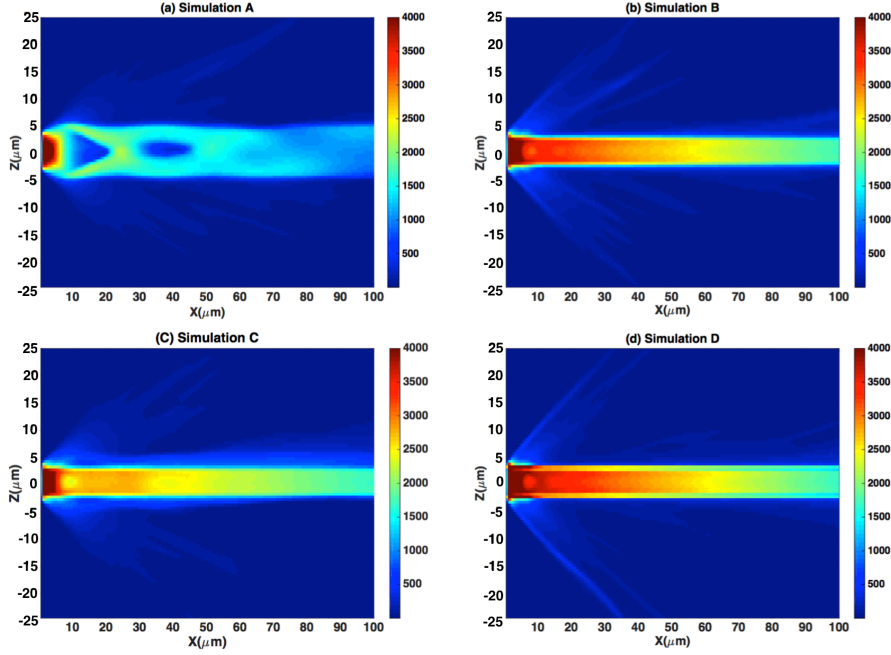


Figure 5: x - z slice of the background temperature (eV) in the y midplane at 2.2 ps for simulations A to D.

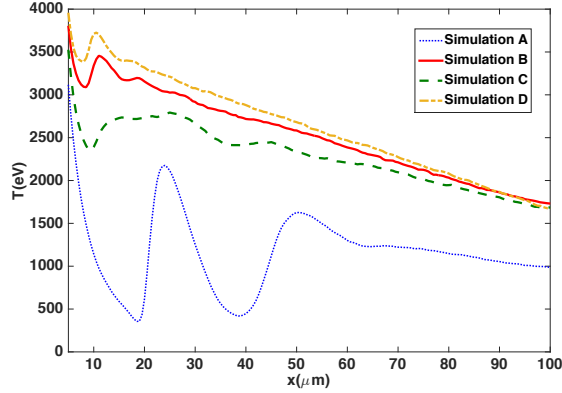


Figure 6: Line-out of the background temperature in eV at 2.2 ps in simulations A to D along x -direction at the centre of y and z .

It is expected that a strong hydrodynamic expansion of the guide and the thermal electron transport into the surrounding material will have significant role on the multi-picosecond timescale. In addition, depending on the choice of different parameters the strong heating of the resistive guide may potentially lead to the generation of strong shocks into the surrounding material⁴. Our simulations only capture the dominant physics in the regime of interest of 1 to few ps timescales where the fast electron can heat the guide before any significant

hydrodynamic motion occurs or thermal transport.

V. DISCUSSION AND CONCLUSION

In this paper, we have investigated the effect of changing resistivity (by changing Z) in cladding layer around the core of a fast electron guide. We find that a cladding layer leads to superior guiding of electrons than in structures with a step-like change in resistivity. We find a linear gradation in Z enhances the growth of resistive magnetic field, leading to improvement in the magnetic collimation. The product $B_\phi L_\phi$ becomes significantly larger with a graded-interface compared to step-like and co-axial resistive guides. The graded-interface configuration is beneficial for four reasons; it helps to collimate the fast electrons uniformly in the core of the guide. Secondly, a larger guide radius is possible using graded interface. This is more tolerant to the laser pointing stability. Thirdly, an increase in the $B_\phi L_\phi$ product early in the electron injection into the guide promotes fast electron confinement. Fourthly, it helps reduce interior magnetic fields. The condition for best performance of the graded interface resistivity cladding is when the ratio between the core of the guide and the laser spot radius is less than 1.

The fabrication of the graded interface resistivity cladding guides is possible using the alloys. Our simulations suggest that improved heating uniformity afforded by a fast electron guide with a graded resistivity cladding is of considerable benefit. Although the fabrication processes are not easy task compared to the step-like resistive guide, the gains obtained from this type of design mean that the fabrication development effort will be worthwhile. The development in micro-scale target fabrication indicates that target fabricators will soon be able to manufacture such targets.

VI. ACKNOWLEDGMENTS

The authors are grateful for the use of computing resources provided by STFC's Scientific Computing Department. RABA would also like to thank the King Saud University, Saudi Arabia for PhD funding. APLR is grateful for support from the ERC via STRUCMAGFAST grant (ERC-STG-2012).

REFERENCES

- ¹A. Bell, J. Davies, and S. Guerin, Phys. Rev. E **58**, 2471 (1998).
- ²A. Robinson and M. Sherlock, Phys. Plasmas **14**, 083105 (2007).
- ³A. Robinson, H. Schmitz, J. Green, C. Ridgers, and N. Booth, Plasma Phys. Control. Fusion **57**, 064004 (2015).
- ⁴A. Robinson, H. Schmitz, and J. Pasley, Phys. Plasmas **20**, 122701 (2013).
- ⁵A. Robinson, M. Sherlock, and P. Norreys, Phys. Rev. Lett. **100**, 025002 (2008).
- ⁶M. Tabak, J. Hammer, M. E. Glinsky, W. L. Kruer, S. C. Wilks, J. Woodworth, E. M. Campbell, M. D. Perry, and R. J. Mason, Phys. Plasmas **1**, 1626 (1994).
- ⁷M. Tabak, D. Clark, S. Hatchett, M. Key, B. Lasinski, R. Snavely, S. Wilks, R. Town, R. Stephens, E. Campbell, et al., Phys. Plasmas **12**, 057305 (2005).
- ⁸A. Robinson, D. Strozzi, J. Davies, L. Gremillet, J. Honrubia, T. Johzaki, R. Kingham, M. Sherlock, and A. Solodov, Nuclear Fusion **54**, 054003 (2014).
- ⁹A. Robinson, H. Schmitz, J. Green, C. Ridgers, N. Booth, and J. Pasley, Phys. Plasmas **22**, 043118 (2015).
- ¹⁰A. Robinson and H. Schmitz, Phys. Plasmas **20**, 062704 (2013).
- ¹¹S. Kar, A. Robinson, D. Carroll, O. Lundh, K. Markey, P. McKenna, P. Norreys, and M. Zepf, Phys. Rev. Lett. **102**, 055001 (2009).
- ¹²B. Ramakrishna, S. Kar, A. Robinson, D. Adams, K. Markey, M. Quinn, X. Yuan, P. McKenna, K. Lancaster, J. Green, et al., Phys. Rev. Lett. **105**, 135001 (2010).
- ¹³J. R. Davies, Phys. Rev. E **65**, 026407 (2002).
- ¹⁴J. Davies, A. Bell, M. Haines, and S. Guerin, Physical Review E **56**, 7193 (1997).
- ¹⁵A. R. Bell, J. R. Davies, S. Guerin, and H. Ruhl, Plasma Phys. Control. Fusion **39**, 653 (1997).
- ¹⁶Y. Lee and R. More, Phys. Fluids **27**, 1273 (1984).
- ¹⁷S. C. Wilks, W. L. Kruer, M. Tabak, and A. B. Langdon, Phys. Rev. Lett. **69**, 1383 (1992).
- ¹⁸M. Sherlock, Phys. Plasmas **16**, 103101 (2009).